

A Novel Complex State Found in the CMR Regime of Models for Colossal Magnetoresistive Manganites

Cengiz Şen,^{1,2} Shuhua Liang,^{1,2} and Elbio Dagotto^{1,2}

¹*Department of Physics and Astronomy, The University of Tennessee, Knoxville, TN 37996*

²*Materials Science and Technology Division, Oak Ridge National Laboratory, Oak Ridge, TN 32831*

(Dated: June 2, 2019)

The colossal magnetoresistance (CMR) state of manganites is widely believed to be caused by the competition between ferromagnetic (FM) metallic states induced by the double-exchange mechanism and insulators with complex spin, charge, and orbital order. Recent computational studies have indeed found a CMR in small clusters precisely near the frontier between those two states at a realistic hole density $x = 1/4$. However, the nature of the insulator has not been fully understood in previous investigations. This insulator must have special characteristics to cause a CMR, otherwise any competition between ferromagnetic and antiferromagnetic states would induce such an effect, which is not the case. In this report, the competing insulator at electronic density $x = 1/4$ and in the CMR regime is studied in detail using the double-exchange two-orbital model with Jahn-Teller lattice distortions on two-dimensional clusters, employing a very careful large-scale cooling down process in the Monte Carlo simulations to avoid being trapped in metastable states. Our investigations show that this competing insulator has a very unexpected complex structure, involving diagonal stripes with alternating regions with FM and CE-like order. The level of complexity of this new state even surpasses that of the recently unveiled spin-orthogonal-stripe states and their associated high degeneracy. Similar results at $x = 1/3$ are also presented. This new state complements the long-standing scenario of phase separation, since the alternating FM-CE pattern appears even in the present study which is carried out in the clean limit. The present and recent investigations are also in agreement with the many “glassy” characteristics of the CMR state found experimentally, due to the high degeneracy of the insulating states involved in the process. Results for the spin-structure factor of the new states are also here provided to facilitate the analysis of neutron scattering experiments for these materials.

PACS numbers: 75.47.Lx, 75.30.Mb, 75.30.Kz

I. INTRODUCTION

The colossal magnetoresistance (CMR) effect of the manganites provides a fascinating example of the collective behavior and unexpected nonlinearities that can emerge in complex materials, such as transition metal oxides, where several degrees of freedom are simultaneously active.^{1,2} Reaching a deep theoretical understanding of the CMR effect is certainly important in the context of Mn oxides, but also to provide a paradigm for rationalizing related complex phenomena, or to predict similar effects, in other materials.³ The current widely accepted scenario to understand the CMR relies on the existence of insulating states competing with the ferromagnetic (FM) metallic state that is caused by the well-known double exchange mechanism.² In addition, particularly in the presence of quenched disorder or other effects such as strain, intriguing nanometer-scale electronic structures have been found in both experimental efforts and theoretical studies.^{1–17}

Considerable progress in the theoretical analysis of the CMR effect was recently reached when the CMR effect was numerically found in a standard two-orbital double-exchange model for manganites at $x = 1/4$ doping, including Jahn-Teller distortions, in the clean limit.^{18,19} The absence of impurities in this study brings the need to fine tune couplings, such as the antiferromagnetic (AFM) superexchange among the t_{2g} electrons, to be close to the

transition from the metal to the insulator at low temperatures. Quenched disorder is known to enhance considerably the CMR effect and avoid the fine tuning of couplings, rendering the presence of the effect more universal. However, it is still an important conceptual issue to study the CMR in the clean limit using finite clusters, even if such a coupling fine-tuning is needed. Such studies would provide ideas on what makes the manganite oxides so special, since very few other complex materials present such a large magnetoresistance effect in so many members of the same oxide family and in such wide ranges of electronic composition and bandwidth. Moreover, a deep understanding of the CMR effect would contribute to new areas of research where manganites play a fundamental role such as oxide heterostructures²⁰ and manganite multiferroics.²¹

There have been two interesting recent conceptual developments in the study of models for manganites in the clean limit that are of relevance for the present effort. As already briefly mentioned, in Ref. 19 a careful study of the conductance vs. temperature, varying the t_{2g} superexchange coupling to interpolate between the FM metal and the AFM insulator at $x = 1/4$, unveiled a clear CMR effect and a first-order magnetic transition that is in good qualitative agreement with experiments. The AFM insulator was characterized as a $C_{1/4}E_{3/4}$ state in Ref. 19 due to the existence in the static spin structure factor of a peak at momenta $(\pi/2, \pi/2)$ which is of-

ten taken as evidence of CE-like states in experimental work. Since the dominant state at $x = 1/2$ is precisely a well-known CE state,² then such an assignment was natural. The second, even more recent, development was presented in Refs. 22 and 23 where surprisingly highly-degenerate diagonal “stripe” phases were reported at special hole densities in the range between 0 and 1/2. These investigations showed that the competing insulators to the FM metal states at intermediate densities are far more complex than previously anticipated, particularly in the range of hole doping which is of the main interest for CMR effects.

In other words, in the limit $x = 1/2$ it has been clearly shown both experimentally and theoretically that robust states of the CE form, displaying spin, charge, and orbital order, are very stable and dominant. In the other limit $x = 0$, there is also clear evidence of an A-type AFM insulator with orbital order that is also very dominant. However, at intermediate hole densities between $x = 0$ and 0.5 it is still not fully clear what kind of competitors to the FM state do emerge from the many active degrees of freedom in manganites. The $C_{1-x}E_x$ states²⁴ are natural candidates, as assumed in Ref. 19, but the recent prediction of a competing spin-orthogonal-stripe (SOS) states at small electron-lattice couplings,²³ as well as the high degeneracy reported in Ref. 22 that was discussed above, are clearly challenging our understanding of this fundamental aspect of the CMR effect. Knowing the properties of the competing insulator state in the CMR regime with accuracy may unveil why this CMR effect occurs in the first place, since it appears that simply having a competition between a FM metal and any AFM insulator is not sufficient to have a CMR effect. The AFM insulator must have special properties that are currently unknown.

Motivated by these recent developments, in the present publication the insulator found in the $x = 1/4$ CMR

regime of Ref. 19 has been further investigated. To our surprise, this insulating state reveals a remarkable complexity that rivals that of the SOS states and their corresponding degenerate states. The CE peak at $(\pi/2, \pi/2)$ that was reported in Ref. 19 certainly is present and confirmed, and in fact the overall insulator does have regions with the characteristic CE zigzag chains. However, and this is the surprising part, the complete state also contains FM regions of equal length size, so the state is a mosaic of CE and FM regions regularly spaced. Both these CE and FM regions form diagonal stripes, that alternate in a ...-FM-CE-FM-CE-... pattern along one diagonal. The SOS states²³ are not as complex since they have the same pattern of spins along the diagonal stripes, albeit spin rotated by 90° degrees. However, the new state reported here mixes two very different states, the CE and FM states, in a combination that is stable in our computer simulations on finite clusters even in the clean limit, namely without the need to have disorder or strain effects to create such nanoscopic phase competition. It is this exotic combination of CE and FM regions that triggers the CMR effect at least in our computational studies. As discussed in the conclusions section of this manuscript, the present results create a variety of additional conceptual questions in manganites, and they show that the level of complexity of these materials, at least within the model Hamiltonian framework and in two-dimensional geometries, is quite unexpected and remarkable.

II. MODEL AND THE MONTE CARLO TECHNIQUE

In this manuscript, the standard two-orbital lattice Hamiltonian for manganites will be studied using two-dimensional finite clusters. In the well-known limit of an infinite-Hund coupling, the model is explicitly defined as:

$$H = - \sum_{\mathbf{ia}\gamma\gamma'\sigma} t_{\gamma\gamma'}^{\mathbf{a}} [\cos(\theta_{\mathbf{i}}/2) \cos(\theta_{\mathbf{i}+\mathbf{a}}/2) + e^{-i(\phi_{\mathbf{i}}-\phi_{\mathbf{i}+\mathbf{a}})} \sin(\theta_{\mathbf{i}}/2) \sin(\theta_{\mathbf{i}+\mathbf{a}}/2)] d_{\mathbf{i}\gamma\sigma}^\dagger d_{\mathbf{i}+\mathbf{a}\gamma'\sigma} + J_{\text{AF}} \sum_{\langle \mathbf{i}, \mathbf{j} \rangle} \mathbf{S}_{\mathbf{i}} \cdot \mathbf{S}_{\mathbf{j}} \\ + \lambda \sum_{\mathbf{i}} (Q_{1\mathbf{i}} \rho_{\mathbf{i}} + Q_{2\mathbf{i}} \tau_{\mathbf{x}\mathbf{i}} + Q_{3\mathbf{i}} \tau_{\mathbf{z}\mathbf{i}}) + (1/2) \sum_{\mathbf{i}} (\Gamma Q_{1\mathbf{i}}^2 + Q_{2\mathbf{i}}^2 + Q_{3\mathbf{i}}^2), \quad (1)$$

where $t_{\gamma\gamma'}^{\mathbf{a}}$ is the hopping amplitude for the e_g orbitals $\gamma = x^2 - y^2$ and $\gamma' = 3z^2 - r^2$ in the \mathbf{a} direction, J_{AF} is the antiferromagnetic coupling between t_{2g} spins on neighboring sites \mathbf{i} and \mathbf{j} of a two-dimensional lattice, and the Q 's are the various Jahn-Teller JT modes (defined in previous literature).² λ is the dimensionless electron-lattice coupling constant, and $\tau_{\mathbf{z}\mathbf{i}} = \sum_{\sigma} (d_{\mathbf{ia}\sigma}^\dagger d_{\mathbf{ia}\sigma} - d_{\mathbf{ib}\sigma}^\dagger d_{\mathbf{ib}\sigma})$ are the pseudo-spin operators defined in Ref. 2. The last term represents the potential (elastic energy) for the distortions, where Γ is the ratio of spring constants

for breathing- and JT-modes. The rest of the notation is standard. Throughout the numerical simulations described below, cooperative lattice distortions are used, where the actual displacements u_i s for the oxygen atoms are the explicit variables in the Monte Carlo sampling, instead of the linear combinations Q_i s that make up the individual Jahn-Teller modes. Note that in our study both the t_{2g} spins and the lattice degrees of freedom are considered classical for simplicity, approximation widely used in previous efforts.²

The Monte Carlo technique used in these simulations have been discussed extensive in the past,² and details will not be repeated here. The procedure to calculate conductances is also standard.²⁵ However, an important improvement that has been employed here and in some recent studies merits a more detailed discussion. In the present study, the cool-down method has been used, rather than a more standard procedure where a particular temperature is chosen and the simulation is run to converge to a particular set of equilibrium configurations. The latter has proved to be problematic in some cases because there may be competing meta-stable states where the Monte Carlo states become “trapped” and this prevents a proper convergence to the true ground state. The cool-down method, described below, is systematic and successful in achieving a better convergence to the ground state, the only problem being the increased CPU time required at the beginning of the process.

The cool-down method starts by selecting a temperature grid. Often a denser temperature grid is chosen at low temperatures for obvious reasons, namely it is in that range that metastability problems are more likely to arise. The simulation starts in practice in our study at a very high temperature $\beta = 3$ with a completely random configuration of the classical spins and oxygen lattice degrees of freedom. As a first step, the system is allowed to thermalize for the first 10,000 MC steps, and measurements are taken during the next 5,000 steps. Then, the temperature is lowered to the next one in the temperature grid, e.g. $\beta = 4$, and the simulation process continues all the way down to $\beta = 300$, with 5,000 steps for thermalization and another 5,000 steps for measurements at each temperature.

In general, the acceptance ratios of the Monte Carlo simulations deteriorate significantly with decreasing temperature. To avoid this problem, the acceptance ratios were monitored during the entire simulation to make sure that they do not fall below a (less than ideal but) reasonable rate ($\approx 10\%$) for the lowest temperature simulated in the calculation, $\beta = 300$. In practice it was observed that a Monte Carlo window of $\Delta = 3/\beta$ is sufficient to guarantee that the acceptance ratios are still reasonable (here the Monte Carlo window denotes the amount by which the oxygen coordinates, and the two angles needed for each classical spin, are modified before the standard Monte Carlo procedure is used to accept or reject the new configuration).

For a fixed set of model parameters (the electron-lattice coupling λ , and the superexchange coupling J_{AF}), the cool-down process alone might still not be sufficient for full convergence. However, many sets of these model parameters were used in the Monte Carlo runs in parallel (employing several computer nodes) and in the end, by mere comparison of energies, it was observed that often for a subset of those model parameters a convergence to the true ground state was found. The existence of a possible new ground state is then confirmed by comparing its energy with those of the neighboring states in the

phase diagram. In short, by monitoring the smoothness of the values corresponding to several Monte Carlo observables when the model parameters are slightly modified, the overall convergence quality of the results can also be monitored.

Once the true ground state for a fixed model parameter set is identified, the process is reversed, and this time a “heat-up” process is carried out, namely the process starts by using an initial configuration which is the properly converged last configuration of the cool-down process at the lowest temperature. This extra process in the end increases the chances that true converged quantities are obtained. The observables at each temperature are calculated at this stage to a good accuracy by running the simulation with an initial configuration borrowed from the last configuration of the heat-up process. At this stage in the simulation, 20,000 Monte Carlo steps for thermalization were used, and another 100,000 steps for measurements, where the measurements are taken at every 5 Monte Carlo steps. All these values of the Monte Carlo parameters and convergence process are kept the same for all the results discussed below, unless otherwise is indicated explicitly.

III. QUARTER DOPING, $x = 1/4$

In this section, the results obtained using a hole doping density $x = 1/4$ are presented. In Fig. 1, the Monte Carlo total energy vs. the superexchange coupling J_{AF} is shown at a low temperature $\beta = 200$ for the case of a moderate electron-lattice coupling λ . In fact, this coupling has been fixed to $\lambda = 1.3$ throughout the simulations at density $x = 1/4$ discussed below, since previous investigations have shown that this value is optimal for the existence of the CMR peak in the resistivity vs. temperature calculations.¹⁹

Three states are here identified as ground states at this particular doping, including the new state that is the focus of the present publication. At small J_{AF} , the ground state is the well-known FM metal induced by the double-exchange mechanism. At large J_{AF} in the range shown in Fig. 1, the ground state is a previously discussed $C_{1/4}E_{3/4}$ type charge-ordered insulator.²⁴ Figure 1 of Ref. 19 shows that this state was previously believed to be the main competitor to the FM metallic state. The main surprise, and main result of this publication, arises at the intermediate superexchange couplings shown in Fig. 1. In this regime, a new state is identified since the slope of the energy curve is different from the two extremes with purely FM or CE characteristics. The intermediate state must actually be a combination of the properties of the two neighboring states, since it is stable in a narrow region between them. In fact, this novel state consists of diagonal FM regions located in real space sandwiched between CE-like zigzag spin arrangements of a similar size in length, as shown in Fig. 2. This new state will be called “FM-CE” in this publica-

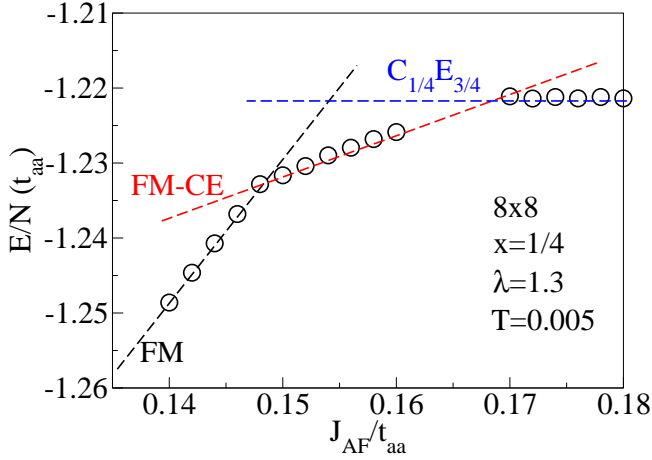


FIG. 1. (color online) Monte Carlo total energy per site vs. J_{AF} for the lowest temperature ($\beta = 200$) used in the cool-down process as described in the text. Other parameters used are as indicated. Circles represent actual Monte Carlo results. Error bars are smaller than the size of the points (not shown).

tion for simplicity. While the FM regions do not display any strong indication of charge ordering, it is clear from the Monte-Carlo snapshots that the CE-like regions are charge-ordered with a checkerboard pattern (see Fig. 2). Note also that the FM regions present an electronic density close to 1 (i.e. $x = 0$), namely close to the undoped limit, while the average density of the CE region is close to $x = 1/2$, rendering the overall density $x = 1/4$. Thus, this state presents a spontaneous nanometer scale phase separation even in the clean limit here investigated.

From many previous theoretical and experimental investigations, it is by now clear that the existence of a CMR relies on a competition between a ferromagnetic metallic state and a charge, spin, and orbitally ordered insulating state.^{2,18,19} The new phase FM-CE unveiled here has all the properties needed for the insulating state, but in addition surprisingly it has a spin ferromagnetic component. As shown in Fig. 3, the calculation of the density of states shows that this new state has a gap at the Fermi level, thus confirming its insulating character. This figure shows the density of states obtained from a Monte Carlo converged state as well as a for an idealized configuration of spins, where the latter is shown both before and after broadening the delta-function peaks using a Lorentzian. In the idealized configuration, the density of states was calculated for a fixed configuration of spins (see Fig. 2), and the lattice variables were not taken into account. Hence, this calculation corresponds to a zero electron-lattice coupling ($\lambda = 0$). This is interesting in the sense that it is known that a finite electron-lattice coupling is needed for the purposes of CMR. While the antiferromagnetic coupling J_{AF} appears sufficient for the stabilization of the spin structure, the electron-lattice coupling stabilizes the charge-ordering characteristics. These calculations show that both couplings play equally important roles to generate the CMR resistivity peak.

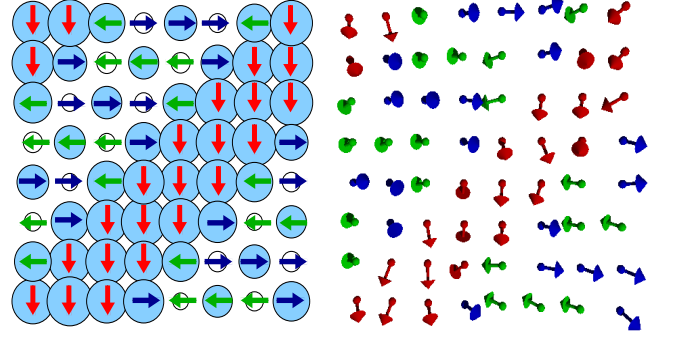


FIG. 2. (color online) Real space representation of the new intermediate state “FM-CE” found at $x = 1/4$. The idealized spin configuration (left) is derived from the actual Monte Carlo converged state (right) obtained at $\lambda = 1.3$ and $J_{AF} = 0.16$. The local charge densities that are depicted with circles in the idealized configuration are taken from the same Monte Carlo snapshot shown on the right. Densities that are $\langle n \rangle > 0.65$ are shown with light-blue filled circles. The largest circle displayed in the figure corresponds to $\langle n \rangle \approx 1$, showing that the ferromagnetically oriented portion of the new state has approximately that density.

The stability of these three states has been studied via calculations of the average carrier density per site $\langle n \rangle$ vs. the chemical potential μ . Figure 4 shows wide plateaus at density $\langle n \rangle = 0.75$ varying μ , at three different couplings representative of the three different states, clearly indicating that all these states are stable in the parameter regions studied in this paper. Also, note that there is another stable region for $\langle n \rangle = 1.25$ (the y -axis in Fig. 4 is normalized to $\langle n \rangle = 2$, the maximum density per site allowed by the two-orbital model), indicative of a possible particle-hole symmetry in the system. It is expected that CMR should also reveal itself for systems that are electron doped, but such a study is beyond the scope of the present publication.

Finally, the resistivity vs. temperature figure obtained in Ref. 19 for the $x = 1/4$ doping is reproduced here to make the discussion and comparison with the new $x = 1/3$ results easier. In the former, the resistivity as a function of temperature displays changes of over a couple of orders of magnitude near the ordering magnetic temperature when parametrized as a function of the superexchange coupling J_{AF} . The location of the resistivity peak coincides nicely with the Curie temperature T_C where the system shows a spontaneous first-order transition to a ferromagnetic state with finite magnetization for the couplings that are close to the phase boundary of the FM metallic state (and a rapid crossover as the distance to the competing insulator increases). The details of these results have been clearly discussed in Ref. 19 and will not be repeated here. It should also be remarked that

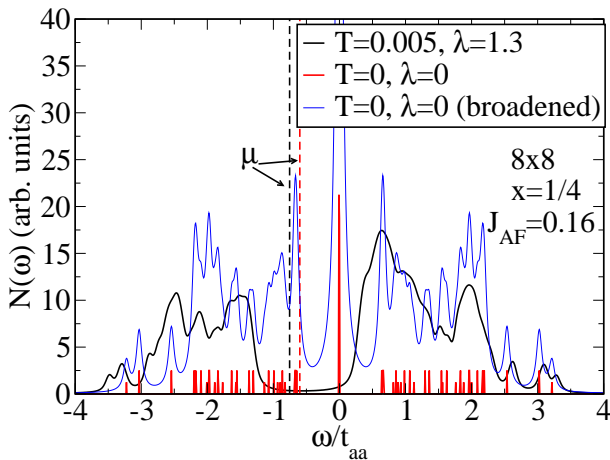


FIG. 3. (color online) Density of states for the new state shown for an idealized ($T = 0$, $\lambda = 0$, fixed spins) and a Monte Carlo converged spin configurations at density $x = 1/4$ ($T = 0.005$, $\lambda = 1.3$). The location of the chemical potential is indicated with μ and it is shown with dashed lines. The density of states and the resistivity calculations (see Fig. 5) confirm that the state at $\lambda = 1.3$ is insulating. The rest of the parameters used are indicated in the figure. Notice that there are states populated at the Fermi level for $\lambda = 0$, at least after broadening, while they are not for $\lambda = 1.3$, giving rise to an insulating state. The sharp peak at $\omega = 0.0$ in the $\lambda = 0.0$ case may correspond to localized states similarly as previously reported in Ref. 19 in the CE states context.

the identification of a new state in this manuscript does not alter at all the transport CMR results of Ref. 19, but here the focus is on the properties of the competing insulating state. An interesting result, as will be discussed in the next section, is that the $x = 1/3$ case actually lacks the resistivity peak that appears in the $x = 1/4$ case, and we will speculate below on the possible differences that might have caused this difference.

IV. ONE-THIRD DOPING, $x = 1/3$

In this section, the similarities and differences between the $x = 1/4$ and $x = 1/3$ hole doping cases will be discussed. In the previous section, a new ground state at $x = 1/4$ doping was identified, which possesses a combination of the properties of the two neighboring ground states, namely, a ferromagnetic and a $C_{1/4}E_{3/4}$ spin-ordered charge-ordered insulating state. This new state “FM-CE” was shown to be an overall insulator, and it seems to be the competitor of the ferromagnetic metallic state that gives rise to the CMR effect.

In the case of the $x = 1/3$ doping, similar calculations were performed but this time using a smaller 6×6 lattice to allow for the $C_{1/3}E_{2/3}$ to properly fit in the cluster analyzed, preventing frustration effects. As a first step in this study at $x = 1/3$, the three-dimensional temperature- λ - J_{AF} phase space was scanned by varying

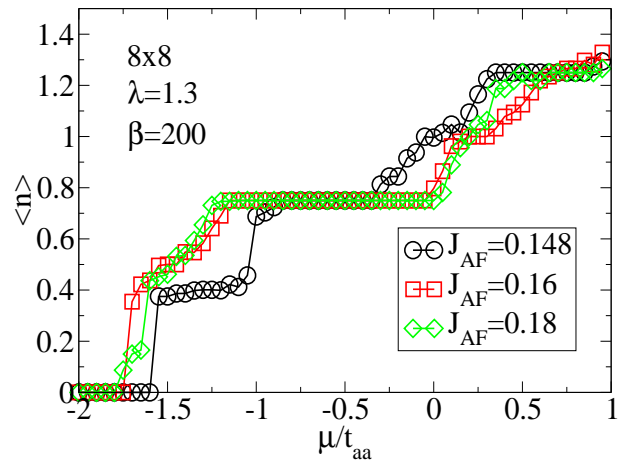


FIG. 4. (color online) Average density vs. chemical potential for the ferromagnetic state, the intermediate new state “FM-CE”, and the $C_{1/4}E_{3/4}$ state, with parameters as indicated in the figure. Note the wide plateau at $\langle n \rangle = 0.75$, suggesting that the intermediate state is quite stable, similarly as the two neighboring states FM and CE. In this calculation, 20,000 Monte Carlo steps were used, where the initial 10,000 steps are discarded for warm-up purposes.

these parameters. Once a clear metal-insulator transition was identified by analyzing the resistivity results, the superexchange coupling was fine-tuned in order to avoid missing a possible delicate CMR physics in the clean limit, which was shown to be the case in the $x = 1/4$ doping. All these calculations were carried out by cooling down the system from high-temperatures, and then heating-up the system where necessary, as explained above. To make sure the ground states have been correctly identified, the Monte Carlo total energy per site E/N vs. the superexchange coupling J_{AF} was monitored at the lowest temperature studied by Monte Carlo, where less than ideal, but still reasonable acceptance ratios (%10 – 15) were obtained. Of course, these acceptance ratios increases significantly to the ideal value of around %50 with increasing temperature.

In Figure 6, the results of E/N as a function of the superexchange coupling J_{AF} are shown for the lowest temperature studied in the simulations, $\beta = 300$. Throughout the simulations that are mentioned in this section, the electron-lattice coupling was fixed to a moderate value $\lambda = 1.1$. This value of λ has been identified as the prospective candidate where CMR physics is expected to happen after the (crude) temperature- λ - J_{AF} phase space analysis was carried out.

The initial cool-down results already indicated a wide J_{AF} region where a new phase was stabilized between the ferromagnetic metallic and the $C_{1/3}E_{2/3}$ states. In order to further improve the results, the last converged configuration of the $J_{AF} = 0.142$ results was used as an input start-configuration for the heat-up results. After this process, the newly identified intermediate J_{AF} region has been shown to be nicely converged, and thus the

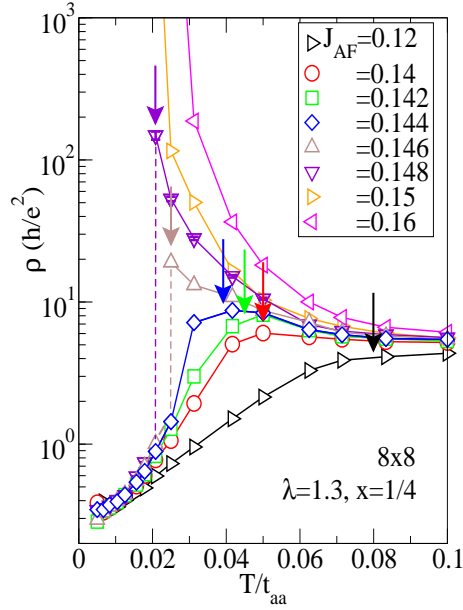


FIG. 5. (color online) Resistivity vs. temperature at $x = 1/4$ doping and moderate electron-lattice coupling ($\lambda = 1.3$) parametrized as a function of the superexchange coupling J_{AF} . A canonical CMR is observed at this doping. The arrows indicate the Curie temperature for ferromagnetism at each value of J_{AF} . This result is reproduced from Ref. 19 to facilitate the comparison in the present manuscript with the $x = 1/3$ results.

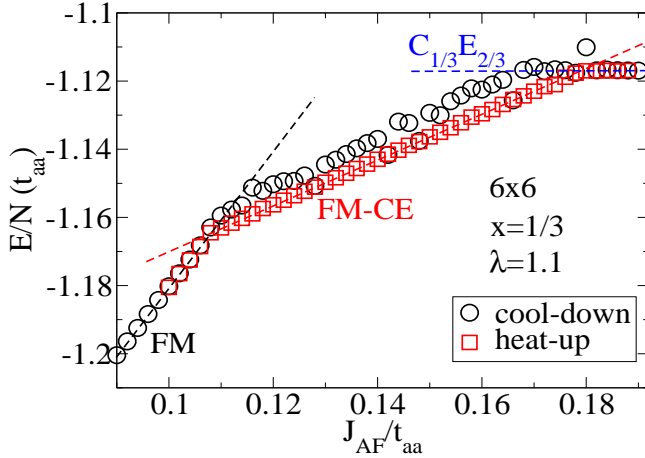


FIG. 6. (color online) Monte Carlo total energy per site vs. J_{AF} for the lowest temperature ($\beta = 300$) used in the Monte Carlo simulations at $x = 1/3$. The initial configuration of the heat-up procedure is taken from one of the converged results of the cool-down simulation, as explained in the text.

existence of a new state at this density is confirmed.

The results from the heat-up procedure were used to sketch the $x = 1/3$ phase diagram as a function of the superexchange coupling J_{AF} that is shown in Figure 7. In each of the two low-temperature phase boundaries the transitions show first-order characteristics (indicated

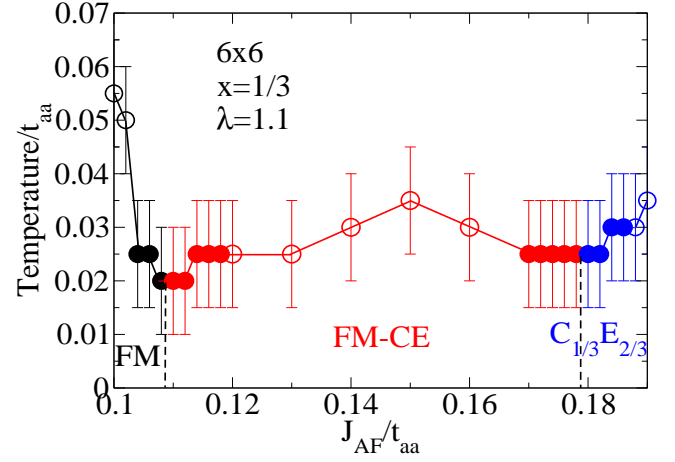


FIG. 7. (color online) Monte Carlo phase diagram corresponding to density $x = 1/3$, obtained employing a 6×6 lattice and the heat-up procedure described in the text. Filled symbols correspond to first-order transitions while open symbols are for second order-transitions, similarly as observed before for the $x = 1/4$ hole density in Ref. 19. Note the presence of first-order transitions both for the cases where the new phase competes with the FM metallic phase, as well as with the $C_{1/3}E_{2/3}$ phase.

with filled symbols in Fig. 7). Away from the phase boundaries, the transitions reveal more common second order characteristics.

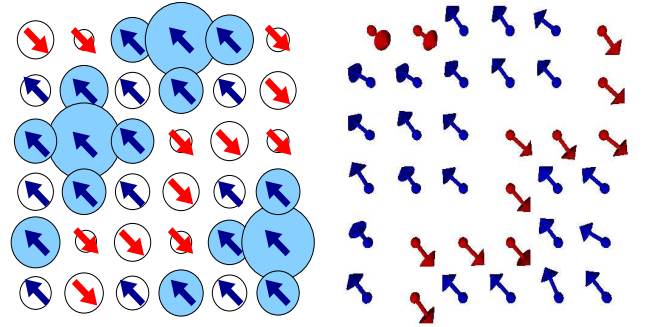


FIG. 8. (color online) Real space sketch of the new intermediate state at $x = 1/3$. The idealized configuration (left) is derived from the actual Monte Carlo converged state (right), for which the parameters are $J_{AF} = 0.166$, $\lambda = 1.1$, and $\beta = 300$. The local charge densities depicted in the idealized configuration are taken from the same Monte Carlo snapshot shown on the right. Densities that are $\langle n \rangle > 0.65$ are shown with light-blue filled circles and the largest circle shown in the figure correspond to $\langle n \rangle \approx 1.25$, appearing in only a few sites.

The real-space Monte Carlo snapshot shown in Figure 8 (b) displays diagonally stacked FM islands separated by a single diagonal CE zig-zag chain. This is to be compared to the spin-ordering of the intermediate state for the $x = 1/4$ case, where similar tendencies were observed. However, unlike in the $x = 1/4$ doping, the diagonal FM regions in the $x = 1/3$ doping show

also a non-uniform charge-ordering pattern. As will be discussed shortly, this seemingly small but obvious difference between the two dopings $x = 1/4$ and $1/3$ may be important to understand the existence of the CMR effect in one case, and the absence of this effect in the other.

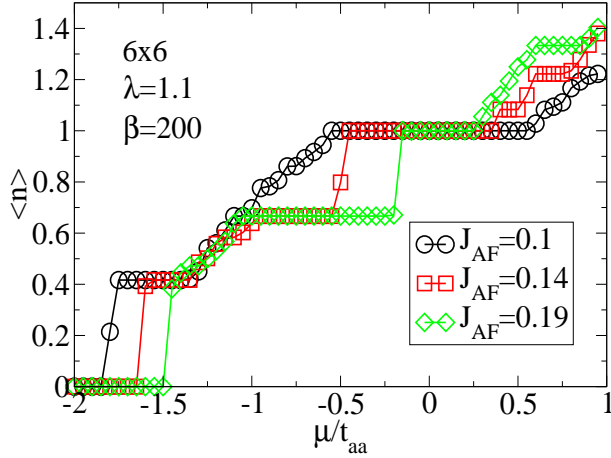


FIG. 9. (color online) Average density vs. chemical potential for the FM, intermediate FM-CE, and $C_{1/3}E_{2/3}$ states with parameters as indicated in the figure. Note that for the new FM-CE intermediate state ($J_{AF} = 0.14$) and the $C_{1/3}E_{2/3}$ state ($J_{AF} = 0.19$) there is a plateau at $n = 0.66$ ($x = 1/3$) showing that the states are stable with a gap, while the FM phase appears to be gapless.

Figure 9 shows the average density as a function of the chemical potential μ , a standard procedure to establish the stability of the three phases that are under investigation here. The $J_{AF} = 0.1$ corresponds to the FM state, whereas $J_{AF} = 0.14$ and $J_{AF} = 0.19$ correspond to the new state and the $C_{1/3}E_{2/3}$ states, respectively. As in the $x = 1/4$ doping case, the latter two in the $x = 1/3$ case are found to be quite stable. Although a plateau is missing in the FM state, the continuity of the average density vs. μ still indicates that FM state is also stable, since a unique μ is sufficient to stabilize the carrier density $x = 1/3$.

In order to further characterize the nature of the new intermediate phase, its density of states was also calculated. Figure 10 shows the results of these calculations for two values of J_{AF} at the same temperature, $\beta = 300$. It is clear that the new state at $x = 1/3$ doping is also insulating similarly as for the new state found at hole density $x = 1/4$.

Finally, the results of the resistivity as a function of temperature are shown at $x = 1/3$ and for several couplings in Fig. 11. The results shown here were reached via the heat-up calculations where the convergence has been shown in practice to be better than just using the cool-down process. Varying the superexchange coupling J_{AF} , this figure clearly shows a metal-insulator transition approximately in the region $0.108 < J_{AF} < 0.11$. A further fine-tuning of the superexchange coupling was not carried out here, since the transition is quite sharp.

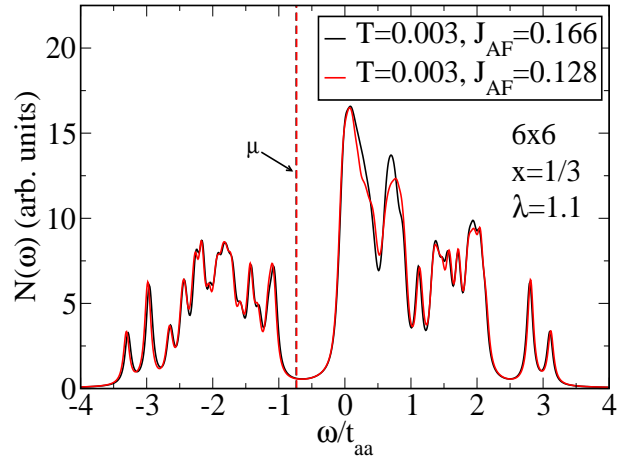


FIG. 10. (color online) Density of states for the new state FM-CE shown for a Monte Carlo converged configuration at density $x = 1/3$. The location of the chemical potential is indicated with μ . Density of states and resistivity calculations confirm that these states are insulating. Parameters used are indicated in the figure.

The main dramatic difference with the $x = 1/4$ results is that a region displaying the CMR resistivity peak is missing. Hence, despite having a well-defined metal-insulator transition, the resistivity peak does not have CMR characteristics at the $x = 1/3$ dopings. This does not prevent a CMR physics to appear when in the presence of quenched disorder, that will smear the sharp first-order characteristics of the resistivity plots, but the focus of this publication is the clean limit. This difference between $x = 1/3$ and $1/4$ will be discussed briefly in the Conclusions and Summary section.

V. SPIN STRUCTURE FACTOR

In this section, the spin-structure factors of the various states discussed here are calculated in order to guide future neutron scattering experiments applied to CMR manganites. For this purpose, here a 24×24 lattice is used, and the spins are fixed to the various C_xE_{1-x} patterns as well as to the two new states discussed in the previous two sections. First, the real-space spin-spin correlations were calculated for various spin pairs averaged over the entire lattice, $(1/N)\langle \mathbf{S}_i \cdot \mathbf{S}_j \rangle$. Then, the spin structure factor $S(\mathbf{k})$ was obtained by simply considering the Fourier transform of the spin-spin correlations:

$$S(\mathbf{k}) = \frac{1}{N} \sum_{\mathbf{i}, \mathbf{j}} \langle \mathbf{S}_i \cdot \mathbf{S}_j \rangle \exp i\mathbf{k} \cdot (\mathbf{r}_i - \mathbf{r}_j), \quad (2)$$

where \mathbf{r}_i is the lattice location of the classical spin \mathbf{S}_i .

To better simulate the experimental situation, where preferred directions in the spin order may not be stabilized due to the formation of multiple domains, the states

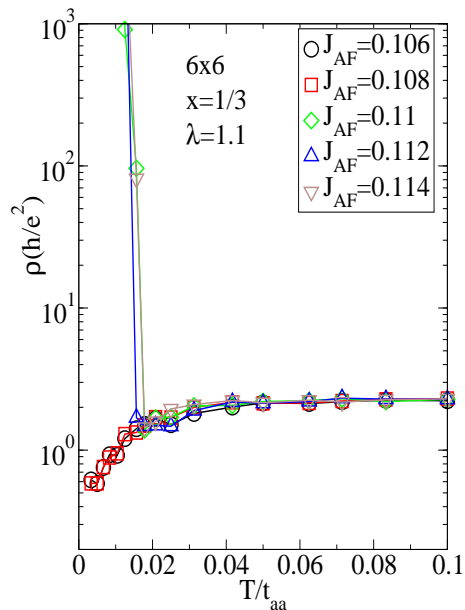


FIG. 11. (color online) Resistivity vs. temperature at doping $x = 1/3$ and for moderate electron-lattice coupling ($\lambda = 1.1$), parametrized as a function of the superexchange coupling J_{AF} . No resistivity peak suggestive of a CMR effect is observed at this doping, contrary to the results found at $x = 1/4$.

under discussion are symmetrized using various rotation and reflection operations. For example, for the simple E -phase, the zigzag chains can be oriented either along the $[11]$ or $[1\bar{1}]$ directions. The symmetry operation to transform one into the other in this case would be a $\pi/2$ -degree rotation either in the clockwise- or counter-clockwise directions. In less trivial cases, such as in the newly found intermediate states, one has two additional states that can be obtained by first rotating the starting state by $\pi/2$ -degree along the z -direction (perpendicular to the layers here investigated), and then taking the reflection of the resulting state along the $[11]$ or $[1\bar{1}]$ directions. All these states could appear in real crystals since they are all energy degenerate, and the average $S(\mathbf{k})$ calculated by averaging over them could be directly contrasted against the results of neutron scattering experiments.

In Figure 12, the spin structure factors for various states are shown in the first quadrant of the Brillouin zone. For the previously studied $C_x E_{1-x}$ states, the dominant peak at $(\pi/2, \pi/2)$ seems to transform into other peaks varying x as shown for the case $x = 1/3$, but those peaks are all along the $(\pi, 0) - (0, \pi)$ direction, as it was discussed in recent publications.²² Thus, if these $C_x E_{1-x}$ states are searched for with neutron scattering the diagonal $(\pi, 0) - (0, \pi)$ must show more intensity than the opposite one $(0, 0) - (\pi, \pi)$.

The new states FM-CE found here display interesting behavior and that merits further discussion. First of all, note that these states not only have peaks along the $(\pi, 0) - (0, \pi)$ direction, induced by the CE component, but also along the other diagonal $(0, 0) - (\pi, \pi)$

direction (although not with the same intensity along the two diagonals). This is to be expected, since the new states possess properties inherited from both the FM state and the $C_x E_{1-x}$ states. While the peaks along the $(\pi, 0) - (0, \pi)$ state are attributed to the $C_x E_{1-x}$ characteristics, the peaks along the $(0, 0) - (\pi, \pi)$ could similarly be attributed to the FM characteristics (with $(0, 0)$ being the characteristic momenta of a long-range uniform ferromagnetic state). These results are actually similar to those reported by Ye *et al.* using neutron scattering experiments.¹⁷ Those experimental results were the first to identify the existence of peaks along the $(0, 0) - (\pi, \pi)$ direction in a single-layer manganite $\text{Pr}_{1-x}\text{Ca}_{1+x}\text{MnO}_4$, for doping levels $x < 0.5$. Their tentative explanation for their findings was expressed in terms of inhomogeneous electronic self-organization, where electron rich domain walls with short-range magnetic correlations are separated from commensurate AF patches.

In our present results an alternative explanation to the results of Ye *et al.*¹⁷ can be envisioned. The notorious peaks along the $(0, 0) - (\pi, \pi)$ direction might very well be due to the existence of the new states reported here that lie in parameter space in between the FM and $C_x E_{1-x}$ states, in the phase diagram varying J_{AF} . It is clear from our $S(\mathbf{k})$ calculations for the intermediate states that, just like as in the neutron-scattering results of Ye *et al.*, the peak that lies in between the $(0, 0)$ and (π, π) peaks has a tendency to move forward in the (π, π) direction as the hole doping is increased from $x = 1/4$ to $x = 1/3$. While it was quite reasonable to explain the neutron scattering results with short-range incommensurate orderings as was done in Ref. 17 using inhomogeneous states, the relevant physics might also be explained via long-range ordering using the intermediate states found in the present manuscript. Further work is needed to better clarify this important aspect of the interpretation of the neutron results.

VI. CONCLUSIONS AND SUMMARY

In this manuscript, the region of the phase diagram where previous investigations¹⁹ unveiled a clear CMR effect in computer simulations has been revisited, with emphasis on the detailed properties of the insulating state that competes with the double-exchange induced FM metal to generate such a CMR effect. In agreement with those previous investigations, this competing insulator is confirmed to have “CE” characteristics with an associated magnetic peak in the spin structure factor $S(\mathbf{k})$ at wave-vector $(\pi/2, \pi/2)$ for hole density $x = 1/4$. However, this insulating state was found to have an unexpected and far more complex structure, since, in addition to CE regions, it also contains FM regions, with the combination having diagonal stripe characteristics that alternate from CE to FM. This exotic structure generates extra peaks in $S(\mathbf{k})$ due to the FM component. The standard $x = 1/4$ CE state, without FM regions, is stabi-

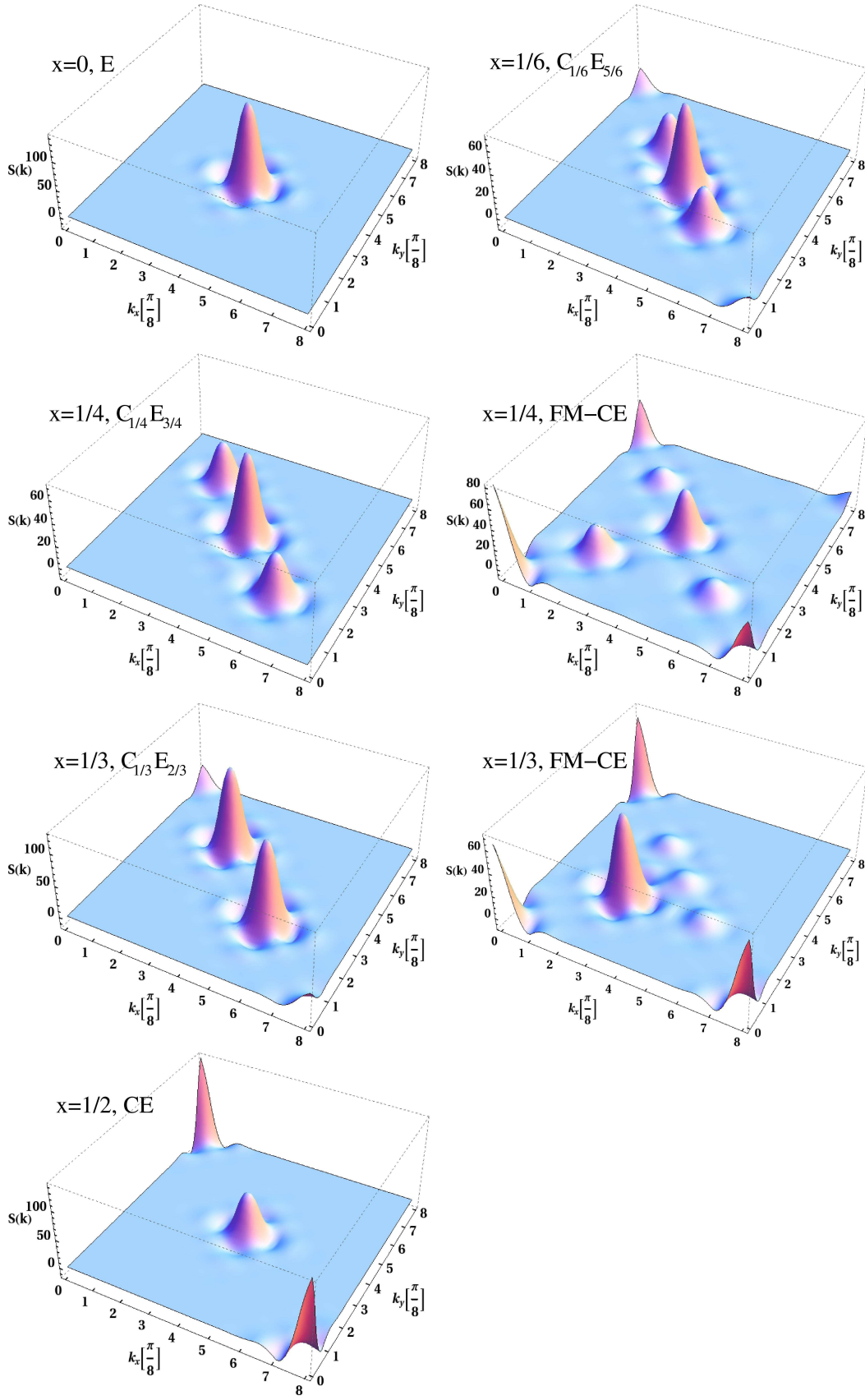


FIG. 12. (color online) The spin structure factors for the various states at the densities indicated in the figure using a 24×24 lattice. For each case, various rotation and reflection operations are used to symmetrize the states, as explained in the text, for better comparison with potential neutron scattering results.

lized upon further increasing the superexchange coupling between the t_{2g} spins. In other words, here it is reported that at $x = 1/4$ and in a narrow region of parameter space, there is a new unexpected phase between the FM metal and the CE insulator, which is a mixture of those two states. It appears that this new state is the competitor of the FM metallic phase that causes the CMR effect in the Monte Carlo computer simulations. Note that the present results are obtained in the clean limit, i.e. without quenched disorder so this new state with mixed characteristics is intrinsic of the standard model for manganites (although it appears in a narrow region of parameter space). Also note that all the previous results presented in Ref. 19 with regards to transport and CMR effects are unchanged and confirmed, the only modification being the characterization of the insulating competing state that is found to be a mixture FM-CE as opposed to just a CE-like state. Finally, about the differences between $x = 1/4$ and $1/3$ with regards to the CMR peak in the resistivity, the only notorious difference between the two FM-CE states at these densities that has been identified at present is that the electronic density in the FM region at $x = 1/4$ appears to be uniform while that at $x = 1/3$ is not. Additional work is needed to understand how this detail can affect the presence or absence of the CMR peak.

There are a few caveats that the reader should be alerted about with regards to the new results presented in this paper. First, states as complex as the one unveiled here with a FM-CE mixture in an alternating diagonal striped pattern are difficult to analyze with regards to finite size effects. The reason is that a size scaling analysis must be carried out only using clusters where the state under discussion fits properly, otherwise frustration effects will complicate the study. The present status of computer simulations of models of manganites prevents such an analysis to be carried out due to growth of the computer effort as N^4 , with N the number of sites, due to the fermionic diagonalizations needed. Thus, the present efforts are restricted to one lattice size only. Second, the study carried out here has been performed using two-dimensional clusters, since a three-dimensional study with the new complex state fitting properly inside cannot be carried out at present again due to the rapid growth of the effort with the number of sites. Then, while our work in principle does apply to single-layer manganites, it is unclear if they can be extrapolated to three dimensions assuming a stacked arrangement of the new state. For this reason is that our predictions for neutron scattering have *not* been compared against available neutron scattering data for the three-dimensional manganites, but it was contrasted only against single-layer neu-

tron results. Third, in this and related efforts it is often assumed that screening effects are sufficient to suppress long-range Coulombic forces. This is usually a reasonable assumption widely used before in model Hamiltonians for manganites, cuprates, and other transition metal oxides. However, the new FM-CE state has nanoscopic regions where the electronic densities seem to be different, i.e. the FM and CE regions do not have the same average electronic density. Thus, another issue that must be studied in future efforts is the stability of the present results against long-range Coulomb repulsion.²⁶

With the caveats previously described, the results presented here suggest a degree of complexity in the study of manganite models that is well beyond previous expectations. The much studied CE state at $x = 1/2$ with simultaneous spin/charge/orbital order in zigzag arrangements was already considered rather exotic in the complex oxide context. The recent theoretical efforts unveiling highly-degenerate states involving diagonal stripes already suggested that this simple picture may be incomplete and hinted toward an even higher degree of complexity with similar patterns that are repeated in a variety of ways along, e.g. one of the diagonals.^{22,23} The present results add a new layer of complexity since now the diagonal stripes alternate between having FM and CE characteristics. This new state far from being a pathology apparently is the key element to induce the famous CMR effect, at least in the computer simulations using finite clusters reported here and in Refs. 18 and 19. Thus, a new avenue may have been opened in the study of manganites that hopefully will locate us closer to understanding these materials and the associated CMR effect. The present effort has revealed a novel unexpected state that was not envisioned before, since it emerges from a nontrivial competition of several tendencies. But much more work is needed to better comprehend these new states and their unusual exciting properties, and how is that they cause the CMR effect.

VII. ACKNOWLEDGMENT

This work was supported by the U.S. Department of Energy, Office of Basic Energy Sciences, Materials Sciences and Engineering Division. The computational effort was supported in part by the National Science Foundation through Teragrid resources under grant number TG-DMR110033. The computations were performed on Kraken (a Cray XT5) at the National Institute for Computational Sciences (<http://www.nics.tennessee.edu/>). This research used the SPF computer program and software toolkit developed at ORNL (<http://www.ornl.gov/~gz1/spf/>).

¹ Y. Tokura, *Colossal Magnetoresistance Oxides* (Gordon and Breach, 2000); M. Salamon and M. Jaime, Rev. Mod.

Phys. **73**, 583 (2001); J. M. De Teresa, M. R. Ibarra, P.

- A. Algarabel, C. Ritter, C. Marquina, J. Blasco J. García, A. Del Moral, and Z. Arnold, *Nature* **386**, 256 (1997); M. Uehara, S. Mori, C. H. Chen, and S.-W. Cheong, *Nature* **399**, 560 (1999); Y. Tomioka and Y. Tokura, *Phys. Rev. B* **66**, 104416 (2002); L. Demkó, I. Kézsmárki, G. Mihály, N. Takeshita, Y. Tomioka, and Y. Tokura, *Phys. Rev. Lett.* **101**, 037206 (2008).
- ² E. Dagotto, T. Hotta, and A. Moreo, *Phys. Rep.* **344**, 1 (2001); A. Moreo, S. Yunoki, and E. Dagotto, *Science* **283**, 2034 (1999).
- ³ E. Dagotto, *Science* **309**, 258 (2005).
- ⁴ J. Burgy, M. Mayr, V. Martín-Mayor, A. Moreo, and E. Dagotto, *Phys. Rev. Lett.* **87**, 277202 (2001); J. Burgy, A. Moreo, and E. Dagotto, *Phys. Rev. Lett.* **92**, 097202 (2004).
- ⁵ J. A. Vergés, V. Martín-Mayor, and L. Brey, *Phys. Rev. Lett.* **88**, 136401 (2002).
- ⁶ S. Kumar and P. Majumdar, *Phys. Rev. Lett.* **96**, 016602 (2006); **94**, 136601 (2005).
- ⁷ C. Şen, G. Alvarez, H. Aliaga, and E. Dagotto, *Phys. Rev. B* **73**, 224441 (2006).
- ⁸ G. Alvarez, H. Aliaga, C. Şen, and E. Dagotto, *Phys. Rev. B* **73**, 224426 (2006).
- ⁹ C. Şen, G. Alvarez, Y. Motome, N. Furukawa, I. A. Sergienko, T. Schulthess, A. Moreo, and E. Dagotto, *Phys. Rev. B* **73**, 224430 (2006).
- ¹⁰ D. S. Dessau, T. Saitoh, C.-H. Park, Z.-X. Shen, P. Vilella, N. Hamada, Y. Moritomo, and Y. Tokura, *Phys. Rev. Lett.* **81**, 192 (1998); A. Moreo, S. Yunoki, and E. Dagotto, *Phys. Rev. Lett.* **83**, 2773 (1999).
- ¹¹ C. P. Adams, J. W. Lynn, Y. M. Mukovskii, A. A. Arsenov, and D. A. Shulyatev, *Phys. Rev. Lett.* **85**, 3954 (2000).
- ¹² D. N. Argyriou, J. W. Lynn, R. Osborn, B. Campbell, J. F. Mitchell, U. Ruett, H. N. Bordallo, A. Wildes, and C. D. Ling, *Phys. Rev. Lett.* **89**, 036401 (2002).
- ¹³ R. Mathieu, D. Akahoshi, A. Asamitsu, Y. Tomioka, and Y. Tokura, *Phys. Rev. Lett.* **93**, 227202 (2004). See also H. Aliaga, D. Magnoux, A. Moreo, D. Poilblanc, S. Yunoki, and E. Dagotto, *Phys. Rev. B* **68**, 104405 (2003) and Y. Motome, N. Furukawa, and N. Nagaosa, *Phys. Rev. Lett.* **91**, 167204 (2003).
- ¹⁴ Y. Tomioka and Y. Tokura, *Phys. Rev. B* **70**, 014432 (2004).
- ¹⁵ E. Božin, M. Schmidt, A. H. DeConinck, G. Paglia, J. F. Mitchell, T. Chatterji P. G. Radaelli, Th. Proffen, and S. J. L. Billinge, *Phys. Rev. Lett.* **98**, 137203 (2007).
- ¹⁶ H. M. Rønnow, Ch. Renner, G. Aeppli, T. Kimura, and Y. Tokura, *Nature* **440**, 1025 (2006).
- ¹⁷ F. Ye, Songxue Chi, J. A. Fernandez-Baca, A. Moreo, E. Dagotto, J. W. Lynn, R. Mathieu, Y. Kaneko, Y. Tokura, and P. Dai, *Phys. Rev. Lett.* **103**, 167202 (2009).
- ¹⁸ C. Şen, G. Alvarez, and E. Dagotto, *Phys. Rev. Lett.* **98**, 127202 (2007).
- ¹⁹ C. Şen, G. Alvarez, and E. Dagotto, *Phys. Rev. Lett.* **105**, 097203 (2010).
- ²⁰ S. Dong, R. Yu, S. Yunoki, G. Alvarez, J.-M. Liu, and E. Dagotto, *Phys. Rev. B* **78**, 201102(R)(2008), and references therein.
- ²¹ S. Dong, R. Yu, S. Yunoki, J.-M. Liu, and E. Dagotto, *Phys. Rev. B* **78**, 155121 (2008), and references therein.
- ²² S. Liang, M. Daghofer, S. Dong, C. Şen, and Elbio Dagotto, *Phys. Rev. B* **84**, 0024408 (2011).
- ²³ S. Dong, R. Yu, J.-M. Liu, and E. Dagotto, *Phys. Rev. Lett.* **103**, 107204 (2009).
- ²⁴ T. Hotta, M. Moraghebi, A. Feiguin, A. Moreo, S. Yunoki, and E. Dagotto, *Phys. Rev. Lett.* **90**, 247203 (2003).
- ²⁵ J. A. Vergés, *Comput. Phys. Commun.* **118**, 71 (1999).
- ²⁶ For some results mixing the double-exchange formalism with Hubbard interactions at the mean-field level see T. Hotta, A. L. Malvezzi, and E. Dagotto, *Phys. Rev. B* **62**, 9432 (2000).